ANALYSIS OF CHARGING DYNAMICS
by C.K. Purvis and R.C. Olsen

In this second of two papers, we analyze the charging results obtained by Olsen and Purvis by means of models which emphasize the importance of surface potential variations (differential charging) in determining the potential of an object. The major effect to be explained is the large difference in the charging frequencies of the two satellites, ATS-5 and ATS-6, and the absence of charging on satellites with conducting surfaces.

The existence of substantial potentials on spacecraft at geosynchronous altitude was established by DeForest (1972) and Whipple (1976) on the ATS-5 and ATS-6 satellites. DeForest was able to explain the large negative potentials seen in eclipse as the natural result of a balance between the currents drawn from the ambient plasma and the currents due to secondary emission from the spacecraft surface. This work followed the form established by Whipple. Garret and DeForest (1978) were able to extend this method of analysis to the entry into eclipse of the ATS satellites, matching the variations in potential to the variations in illumination. An implicit assumption of this work was that the spacecraft was in equilibrium at each moment, that is, the time constant for a charging balance was considerably less than the time period for variations in illumination. This analysis worked reasonably well for the ATS eclipse events.

ATS-6, and to a lesser extent, ATS-5, also charged to substantial negative potentials in sunlight. Given the substantial photoelectric current, compared to the ambient currents, it was not possible to explain the daylight charging process in terms of a simple current balance. The suggestion by Whipple (1976) that differential charging on the surface of ATS-6 might be responsible for an observed barrier to electron motion provides the necessary clue for the solution of the problem.

The next step in the analysis was to identify the differentially- charged surface(s).

A three-dimensional computer code, NASCAP, was successfully applied to the ATS-6 charging observations in equilibrium. This analysis showed that the barrier observed by the UCSD particle detectors was due to the parabolic dish antenna below the experiment package. (Olsen, McIlwain, and Whipple,1981.) This large insulating surface was capable of charging negatively with respect to the mainframe, and causing an electrostatic barrier around the EME package on the top of the spacecraft. It is not clear that this insulating surface is the dominant one in the total current balance of the spacecraft, since a large portion of the spacecraft conducting area is on the EVM away from the antenna. Having established the existence of differential charging on ATS insulating surfaces, we now proceed to the development of models which can be used to interpret the observed charging dynamics.

It was noted that one-dimensional current balance models, as developed by Whipple (1965) and DeForest (1972), and used by Prokopenko and Laframboise((1980) can successfully be used to interpret regular eclipse charging events. These models also

imply that shadowed insulating surfaces on a sunlit spacecraft may charge negatively. These models do not address the question of daylight charging as observed on ATS-5 and -6. The three-dimensional charging model, NASCAP, provides the necessary tool to begin answering questions about the causes of daylight charging. Mandell et al., (1978) applied this model to the idealized case of a teflon sphere in a Maxwellian environment, illuminated on one side. They showed that a negative potential on the shadowed side would develop relatively quickly, and that the resulting electrostatic fields would cause a barrier to develop around the illuminated portions of the sphere. Once the barrier to electron motion was established, the photoelectric current from the illuminated surfaces was reduced, and eventually cut off. This allowed the front surfaces to charge negatively, and the entire object charged negatively thereafter.

The complexity of NASCAP, which was designed as an engineering tool, makes its application to the study of physical processes difficult at times, and a pair of severely idealized models have been developed to study the static barrier and time dynamics of differential charging processes. The first effect will be studied with an insulating sphere which has a monopole plus dipole electric field imposed upon it. The time dynamics effects will then be addressed with an object composed of two (conducting) hemispheres and an ad hoc barrier effect taken from the monopole plus dipole model. We will then return to the NASCAP model, mainly to compare the differences between a spinning satellite (ATS-5), and a three-axis-stabilized one (ATS-6).

MONOPOLE PLUS DIPOLE MODEL
Besse and Rubin (1980) showed that the concept of a barrier could be illustrated by using a spherical object with a monopole plus dipole potential distribution imposed. This idea is extended here to include the effects of particle trajectories on the barrier that would be observed from the surface of the sphere, and the effects it would have on thermal electron currents.
The model uses a spherical object with cylindrical symmetry, and a surface potential given by:

$\Phi(R,\theta) = V_m + V_d \cos(\theta)$
where:
R = sphere radius,
V_m = monopole voltage = the potential at the center of the sphere,
V_d = dipole voltage = the potential difference between the top and center
θ = the angle from the z-axis

These terms are similar to but not identical to the first two terms in a multipole expansion of an arbitrary potential distribution. The monopole potential is the average over the sphere, the dipole potential is half the differential potential from top to bottom.

The potential away from the sphere is:
$$\Phi(r,\theta) = V_m (R/r) + V_d \cos(\theta) (R/r)^2$$
A potential minimum will develop outside the sphere at
$R_m = -2R (V_d / V_m) \cos(\theta)$

if the combination of signs is positive. The potential on the positive z-axis at this point is:

$$\Phi(Rm, A = 0) = -25\, V_m^2\, /\, V_d$$

For the physical cases considered in this work, V_d is always positive, so for a barrier-to form above the sphere, Vm must be negative. Also, for the radius to be greater than R, we must have: $2\, V_d > (-V_m)$

The monopole potential here is the averaged potential over the sphere, and V_d is half the top to bottom difference, so we see that this condition is that the differential potential be of greater magnitude than the average potential. This condition can lead to abrupt changes in the barrier height for relatively small changes in the sphere potential distribution.

Also, if a differentially charged object enters eclipse, the differential potential may be maintained as the spacecraft charges (more) negative, but the barrier may disappear.

The barrier height to electron motion along the z-axis which results from this potential minimum is the difference between the potential at the top of the sphere and the minimum:

$$V_b = 0.25\, V_m^2 /\, V_d + (V_m + V_d)$$
$$= (V_m + 2\, V_d)^2 /\, (4\, V_d)$$

Because of the difference in the sign of V_m and V_d, it is possible to have large sphere potentials, but a small barrier.
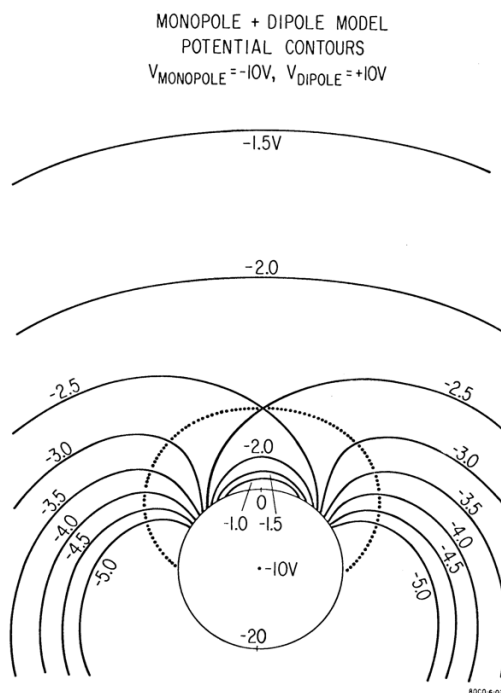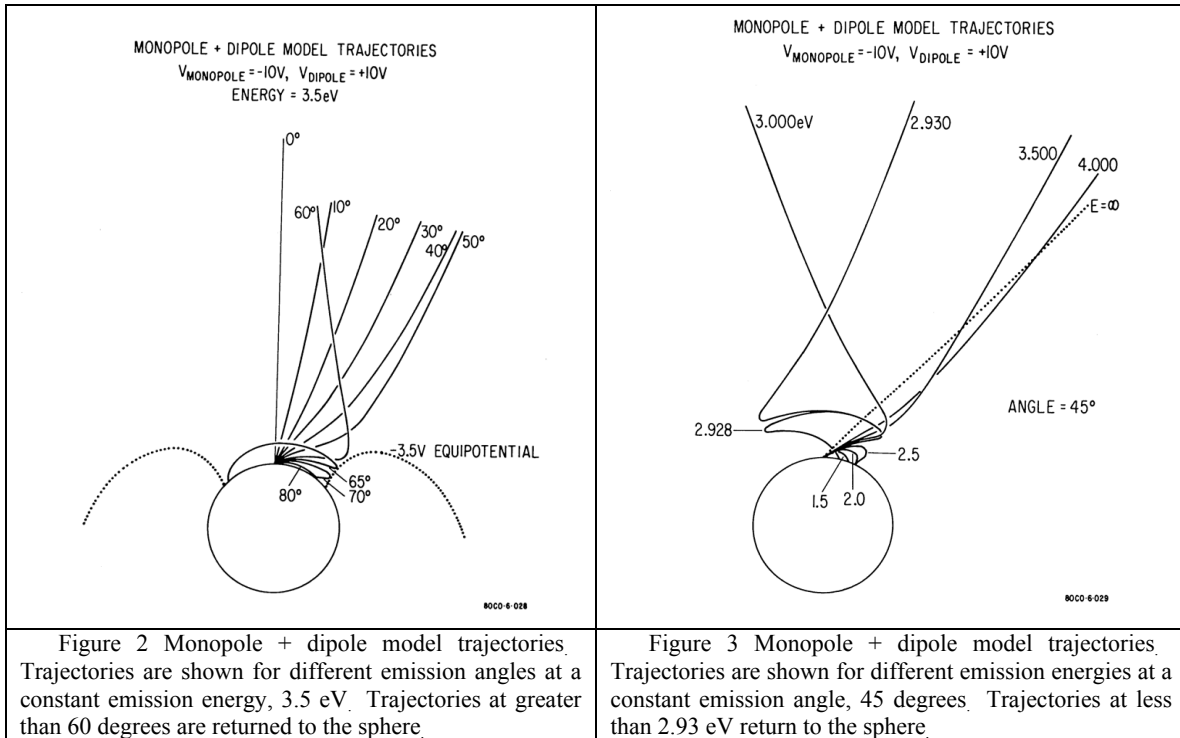

Figure 1 Monopole + dipole model potential contours. The spherical (circular) surface is the inner boundary where the potential distri- bution is specified, the solid lines outside are the equipotentials. The dotted line is the potential minimum along rays from the top of the sphere. There is a saddle point at -2.5 V above the top of the sphere.
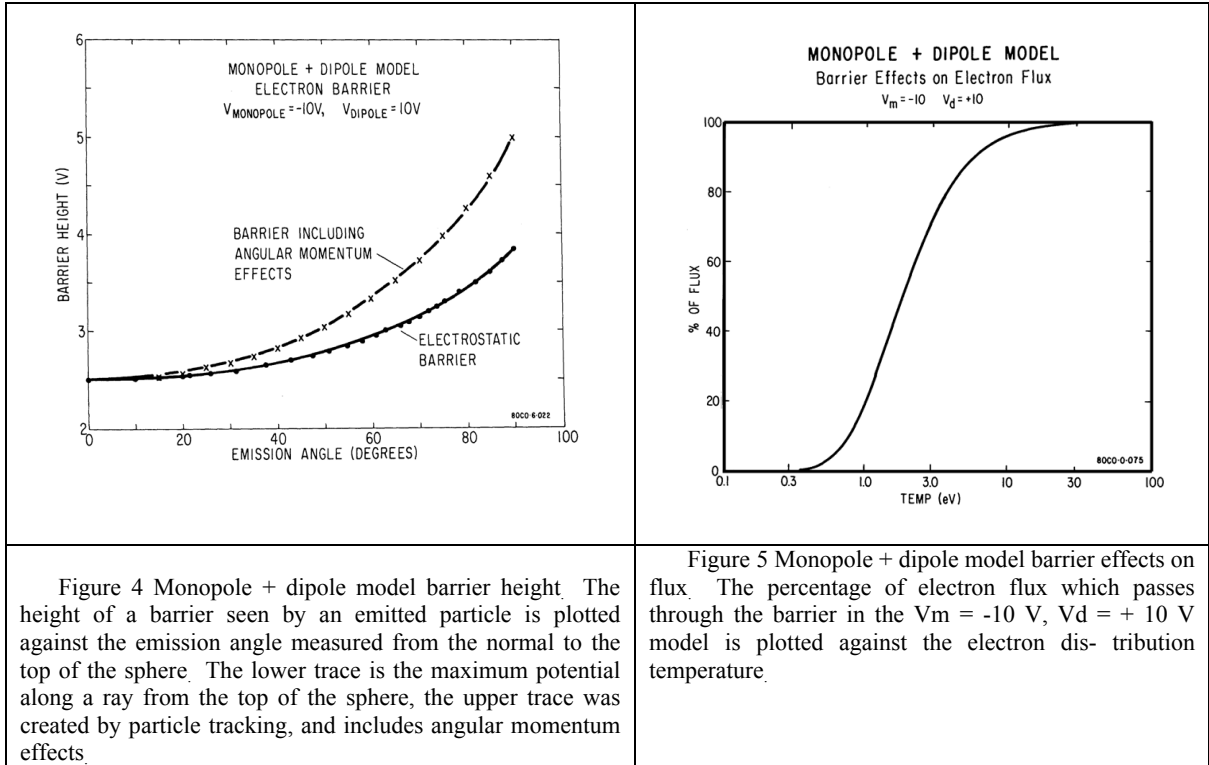

An example of the effects of differential charging is developed beginning with Figure 1. Potential contours are shown for the case of a monopole potential of -10V, and dipole potential of +10V. This results in a potential at the top of the sphere of 0 V, and -20 V at the bottom. There is a symmetry about the z-axis, and a rough spherical symmetry outside 2 sphere radii and above -2.5 V. Inside two sphere radii, the dipole potential dominates. There is a saddle point on the z-axis, at the 2 radius point, with a potential of -2.5 V. This would be a 2.5 V barrier to electron motion along the z-axis. The dotted line is the locus of potential minima as seen along rays from the top of the sphere. The potential values along this locus are plotted versus ray angle in Figure 4, to be discussed shortly. The effects of the potential distribution on particle motion can be quite large, as demonstrated by the next pair of figures. Figure 2 shows the particle trajectories

calculated for the potential distribution shown in Figure 1. Particles are emitted from the top of the sphere at various angles, with an energy of 3.5 eV. Bending of the particle trajectories causes particles emitted at angles greater than 63° to be returned to the surface of the sphere. These latter particles reverse their motion at the 3.5 eV equipotential. Figure 3 shows the particle trajectories for particles emitted at 45°, with varying energies. The critical energy for escape in this case is 2.93 eV. In both figures, it is clear that trajectories near the critical value are extremely distorted.

| Figure 2 Monopole + dipole model trajectories. Trajectories are shown for different emission angles at a constant emission energy, 3.5 eV. Trajectories at greater than 60 degrees are returned to the sphere. | Figure 3 Monopole + dipole model trajectories. Trajectories are shown for different emission energies at a constant emission angle, 45 degrees. Trajectories at less than 2.93 eV return to the sphere. |

The importance of trajectory effects in determining the barrier height is illustrated in Figure 4. The potential height seen for motion along a ray is plotted in the lower curve, labeled electro- static barrier. The upper curve includes angular momentum effects, and was determined by tracking particles. Olsen, et al., showed that this model successfully duplicated the observed angular dependence of the ATS-6 electrostatic barrier.

Finally, Figure 5 shows the effect such a barrier would have on an emitted flux of electrons, as a function of the temperature of the electron population. (This would also apply to electron fluxes inward.) The emission point is still at 0 V, and we are looking entirely at barrier effects. Only 20% of the flux escapes for a 1 eV population, with some 50% escaping by 1.8 eV. A photoelectron population will have a temperature in this range, and we see that a small potential difference ($V_d = 10$ V) can cause large effects on the net current to the sphere.

Figure 4 Monopole + dipole model barrier height. The height of a barrier seen by an emitted particle is plotted against the emission angle measured from the normal to the top of the sphere. The lower trace is the maximum potential along a ray from the top of the sphere, the upper trace was created by particle tracking, and includes angular momentum effects.

Figure 5 Monopole + dipole model barrier effects on flux. The percentage of electron flux which passes through the barrier in the Vm = -10 V, Vd = + 10 V model is plotted against the electron dis- tribution temperature.

TWO-HEMISPHERE MODEL

Given an effective method of shutting off the photoelectric current, the charging dynamics become clear. To study this effect a simple computer model composed of two conducting hemispheres was created. The hemispheres are connected by a capacitor, and have a capacitance to the distant plasma. The top hemisphere has an electron source associated with it, which combines with thermal plasma currents and secondary currents to charge the hemispheres. The barrier is added in an ad hoc manner by applying the monopole plus dipole results. The barrier height for the electron source is taken as the barrier which would be obtained if the potentials on the hemispheres were those of the top and bottom of an insulating sphere. This model allows us to examine the two main characteristics which determine daylight charging - barrier effects and the capacitance between insulating surfaces and underlying substrates. This form will also allow us to study the quasi- equilibrium of the barrier height.

The object has a radius of 1 meter, and an intrinsic capacitance to the distant plasma of 112 pf. The differential capacitance was set at 5.6×10^4 pf for most runs. Photoelectrons were modeled as 1 or 2 eV Maxwellian distributions giving a current of 100 μA.
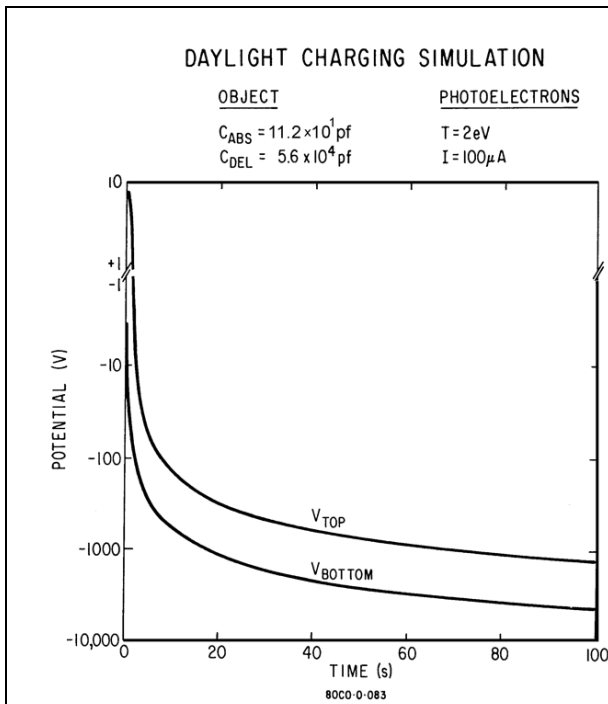

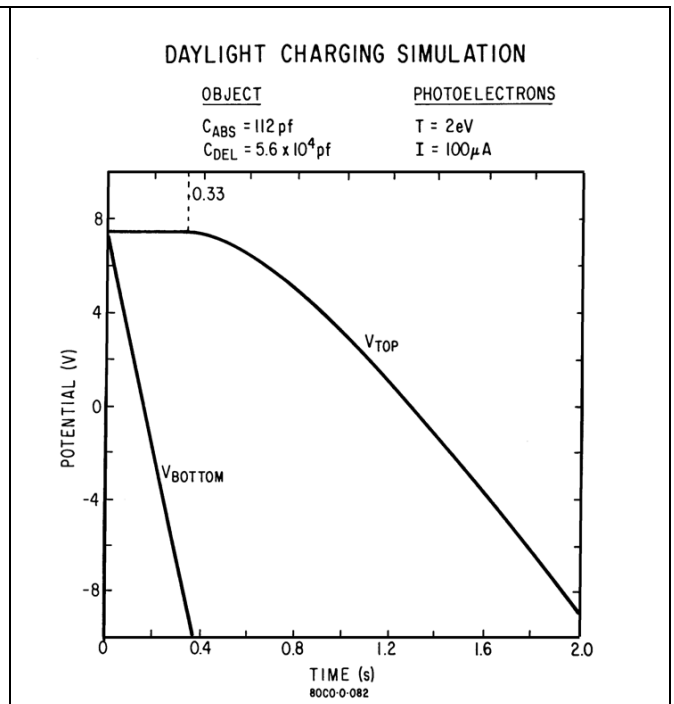| Figure 6 Daylight charging simulation, two hemisphere model. The potential is plotted versus time on a log-linear scale, with the potential broken at + 1 V. | Figure 7 Daylight charging simulation potential plot. The data in Figure 6 are plotted with a linear potential scale for the first two seconds of the simulation. The potential of the top hemisphere begins to drop at .33 seconds. |

A number of computer runs were made, all with essentially the same results. A typical case is shown in Figures 6 to 8. An initial state with both hemispheres positive (7.4 V for 2 eV electrons) in a 10 keV Maxwellian plasma was an equilibrium.

Only a small fraction of the emitted "photoelectrons" escaped at any time. The initial positive potential fulfilled the role taken later by the differential potential. The negative charging of the bottom hemisphere was hindered by the "large" capacitance, and slowly charged negative, while the top remained positive. After a short time both began to drop together, but with the bottom hemisphere always leading.

Figure 6 shows this 'behavior over the modeled period. We see that the charging rate is not constant, nor is an equilibrium potential reached by either hemisphere.
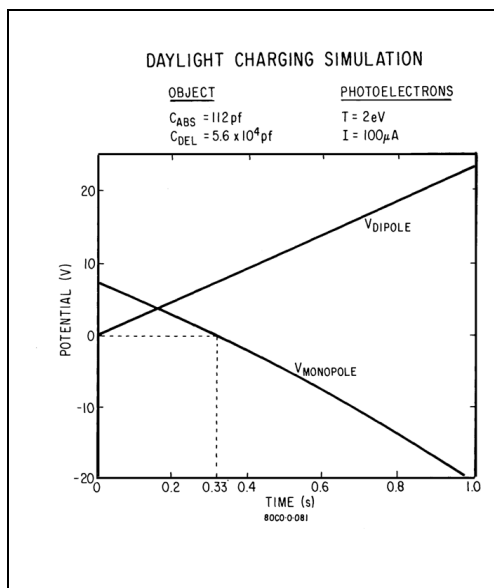

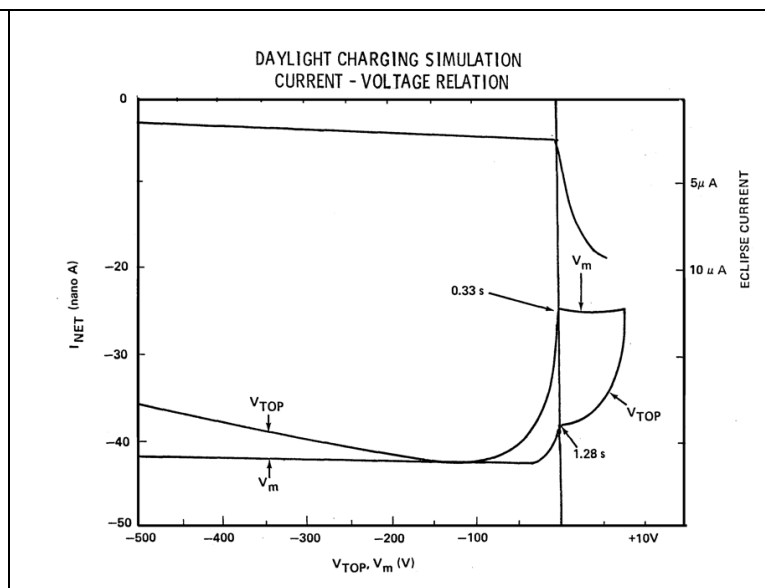| Figure 8 Daylight charging simulation potential plot. The monopole and dipole potentials of the case in Figures 6 and 7 are plotted on a linear time scale for the first second of the simulation. The monopole potential crosses the 0 V level at .33 seconds.	Figure 9 Daylight charging simulation, two hemisphere model. The current voltage relationship during the charging run is presented here. The current to the sphere is plotted against the potential of the top hemisphere (V_{top}) and the monopole potential (V_m) Note the change in scale at 0 volts on the potential axis. The upper curve, with its own current scale, on the right, is the current voltage relationship for this object in eclipse.

The curious thing is that the barrier height remains constant. (Not shown because figure is dull.) Here we are referring to the combined effects of the hemisphere potential and any limiting fields. This condition is in fact an equilibrium condition, as becomes clear when we examine the first two seconds of the run more closely. Figure 7 expands the data of Figure 6, and shows us that the top hemisphere remains at a constant positive potential for the first 0.33 seconds. Figure 8 shows that this time is significant because it is the time when the average potential drops below zero, allowing the electrostatic barrier to form. Since differential charging can now supply the necessary barrier to photoemission, the top hemisphere begins to drop in potential.

The matter of a constant barrier height, as indicated by this model, and the ATS-6 particle data, is the major feature which results from this part of the study. We have developed a new equilibrium, consider- ably different than that which would be achieved by a conducting spacecraft. The claim that this is an equilibrium implies that the potentials are stable against small perturbations.

To illustrate this, we return to the case shown in Figures 6 to 8, and perturb the average potential (i.e. V_m) of the object slightly, as might occur if the environment varied briefly. (Changes in V_d will be resisted by the large differential capacitance.)

Varying V_m while holding V_d constant has the effect of changing the barrier height, which alters the current balance of the object. We will see that these changes in current are such as to restore the barrier. Figure 9 shows the current-voltage relationship through the first few seconds of the charging run just shown. The current is plotted against the voltage of the top hemisphere (as might be appropriate for ATS-6) and the monopole voltage (i.e. the average potential). We see that the curve is not monotonic, dipping substantially around -50 V (V_{top}), and then climbing slowly upwards. The current also climbs as a function of the monopole potential, but it is not as obvious over the short time period the -100 to -500 V line represents. On the upper portion of the curve, the current voltage relation for this object in eclipse is shown. Substantially higher net currents flow, and the time scale for charging is appropriately faster, as is observed in eclipse. Looking finally at the claim of equilibrium, we perturbed the potentials on the object, and watched as the object reestablished an equilibrium.
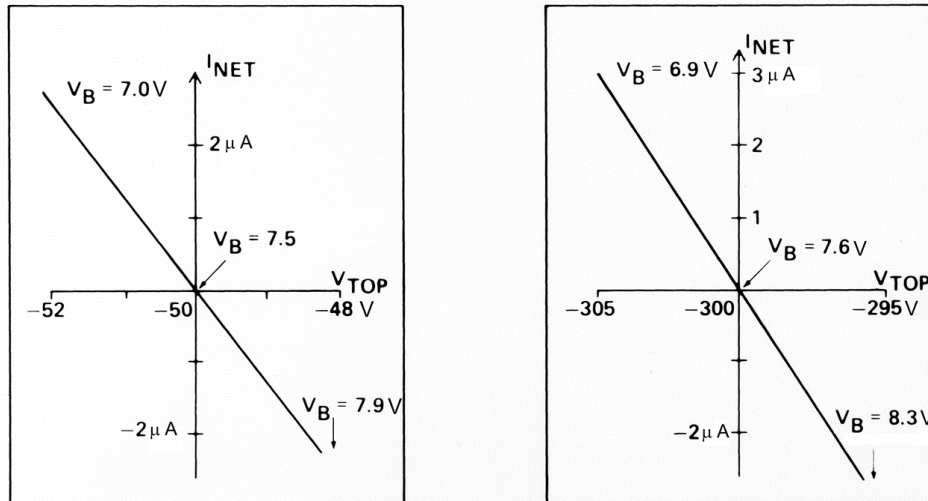

Figure 10 Daylight charging simulation, differential current-voltage relationship. The results of varying the average potential about the values found in Figure 9 are presented here. Arrows indicate the time direction of changes in the potential and current. VB is the barrier height found for the electrostatic barrier over the top hemisphere.

Figure 10 shows what happened when the equilibrium at -50 V and -300 V (top hemisphere) was charged by a few volts. The differential potential was maintained as a constant, as would be expected. This causes the barrier height to change, and therefore major differences in current. These changes are such as to reestablish the initial values. Figure l0a shows the values for a -50 V initial value, perturbing the potential by 2 volts in either direction causes a net current of 2 microamps to flow, several orders of magnitude larger than the net current which is charging the system. Figure 10b shows a similar result for a -300 V initial value, with a 5 volt perturbation. Again, several microamps flow, and equilibrium is regained in a millisecond.

We see that the equilibrium condition of the sphere is to maintain the barrier height at a value where the net current is a small percent- age of the currents in the system. A positive current flows to the top hemisphere, a negative current to the bottom, and a small net negative current to the system as a whole. As this small current builds the differential potential, the system as a whole is allowed to slowly charge negative.

The NASCAP model is now used to complete our study, and show how a spinning satellite is more difficult to charge than a three-axis stablized spacecraft. This is in response to the disparities in charging rates of the two ATS's.

FIGURES